Core-softened fluids, water-like anomalies, and the liquid-liquid critical points

Cite as: J. Chem. Phys. **135**, 044517 (2011); https://doi.org/10.1063/1.3613669
Submitted: 04 March 2011 . Accepted: 28 June 2011 . Published Online: 29 July 2011

Evy Salcedo, Alan Barros de Oliveira, Ney M. Barraz, Charusita Chakravarty, and Marcia C. Barbosa

Core-softened fluids, water-like anomalies, and the liquid-liquid critical points

Evy Salcedo,[1,a)] Alan Barros de Oliveira,[2,b)] Ney M. Barraz, Jr.,[3,c)]
Charusita Chakravarty,[4,d)] and Marcia C. Barbosa[5,e)]
[1]*Departamento de Física, Universidade Federal de Santa Catarina, Florianópolis, SC, 88010-970, Brazil*
[2]*Departamento de Física, Universidade Federal de Ouro Preto, Ouro Preto, MG, 35400-000, Brazil*
[3]*Programa de Pós-graduação em Física da UFRGS, Bento Gonçalves 9500, 91501970, Porto Alegre, RS, Brazil*
[4]*Department of Chemistry, Indian Institute of Technology-Delhi, New Delhi 110016, India*
[5]*Instituto de Física, Universidade Federal do Rio Grande do Sul, Porto Alegre, RS, 1501-970, Brazil*

(Received 4 March 2011; accepted 28 June 2011; published online 29 July 2011)

Molecular dynamics simulations are used to examine the relationship between water-like anomalies and the liquid-liquid critical point in a family of model fluids with multi-Gaussian, core-softened pair interactions. The core-softened pair interactions have two length scales, such that the longer length scale associated with a shallow, attractive well is kept constant while the shorter length scale associated with the repulsive shoulder is varied from an inflection point to a minimum of progressively increasing depth. The maximum depth of the shoulder well is chosen so that the resulting potential reproduces the oxygen-oxygen radial distribution function of the ST4 model of water. As the shoulder well depth increases, the pressure required to form the high density liquid decreases and the temperature up to which the high-density liquid is stable increases, resulting in the shift of the liquid-liquid critical point to much lower pressures and higher temperatures. To understand the entropic effects associated with the changes in the interaction potential, the pair correlation entropy is computed to show that the excess entropy anomaly diminishes when the shoulder well depth increases. Excess entropy scaling of diffusivity in this class of fluids is demonstrated, showing that decreasing strength of the excess entropy anomaly with increasing shoulder depth results in the progressive loss of water-like thermodynamic, structural and transport anomalies. Instantaneous normal mode analysis was used to index the overall curvature distribution of the fluid and the fraction of imaginary frequency modes was shown to correlate well with the anomalous behavior of the diffusivity and the pair correlation entropy. The results suggest in the case of core-softened potentials, in addition to the presence of two length scales, energetic, and entropic effects associated with local minima and curvatures of the pair interaction play an important role in determining the presence of water-like anomalies and the liquid-liquid phase transition. © *2011 American Institute of Physics*. [doi:10.1063/1.3613669]

I. INTRODUCTION

Water is characterized by well-known thermodynamic and kinetic liquid-state anomalies; for example, the rise in density on isobaric heating (density anomaly) and the increase in molecular mobility on isothermal compression (diffusivity anomaly).[1] Since the anomalies of bulk water are connected with its behavior as a solvent in chemical and biological systems, an understanding of the structural origins of such anomalous behavior has attracted considerable attention.[2,3] While the anomalies of water were initially presumed to be uniquely connected to the hydrogen-bonded network of water,[4] there is now evidence that a number of liquids display water-like liquid-state anomalies, such as Te,[5] Ga, Bi,[6] S,[7,8] $Ge_{15}Te_{85}$,[9] silica,[10–12] silicon,[13] and BeF_2.[10,11,14,15] The generic relationships between structure, entropy and mobility underlying this diverse set of liquids with water-like anomalies, can be understood in terms of the behavior of the excess entropy (S_{ex}), defined as the difference between the entropy (S) of the liquid and the corresponding ideal gas at the same density and temperature.[11,16–23] A necessary condition for the fluid to show density, diffusion, and structural anomalies is the presence of anomalous excess entropy behavior, corresponding to a rise in S_{ex} on isothermal compression ($\partial S_{ex}/\partial \rho > 0$).[11,14,15,21–25] The structural basis for the excess entropy anomaly is the existence of distinct forms of local order or length scales in the low- and high-density regimes; competition between the two types of local order results in a rise in excess entropy at intermediate densities.

In addition to the singularity-free scenario for water-like thermodynamic and kinetic anomalies, it has been conjectured that the anomalies of water are due to the presence of a second liquid-liquid critical point, corresponding to the onset of a line of first-order phase transitions between

[a)]Electronic mail: esalcedo@fsc.ufsc.br.
[b)]Electronic mail: oliveira@iceb.ufop.br.
[c)]Electronic mail: neybarraz@gmail.com.
[d)]Electonic mail: charus@chemistry.iitd.ernet.in.
[e)]Electronic mail: marcia.barbosa@ufrgs.br.

high- and low-density phases of water.[26] The relationship between the liquid-liquid critical point and water-like anomalies can be addressed by considering minimal models of liquids with isotropic, pair-additive interactions that give rise to water-like anomalies, as well as liquid-liquid critical points.[27–30] Such simple models are able to capture several water features, including liquid-liquid phase transition, thermodynamic, and dynamic anomalies,[31–35] yet amenable analytically.[36–39] While two length scales in the pair interaction appears to be a necessary condition for seeing both the liquid-liquid critical point (LLCP) and water-like anomalies, it is possible to design isotropic potentials with two length scales where appropriate variation of parameters can result in shifting either the LLCP or the water-like anomalies into the metastable or unstable regime.[40] In this paper, we study a family of liquids with continuous and core-softened pair interactions consisting of a hard core, a short-range shoulder, and an attractive well at a larger separation.[40] Since the potentials share a common functional form consisting of a sum of one Lennard-Jones and four Gaussian terms, we refer to them as the family of multi-Gaussian water-like liquids. By suitably varying the parameters, the outer attractive well can be left unchanged, while the shoulder can be progressively altered from being purely repulsive to a deep attractive well. As the shoulder shifts from being purely repulsive to more attractive, the anomalous regime in the pressure-temperature plane shrinks and disappears while the LLCP shifts to higher temperatures and lower pressures. The connection with atomistic models is made by ensuring that the limiting case of the double minimum potential that has no anomalies corresponds to an isotropic potential that reproduces the oxygen-oxygen radial distribution function of ST4 water.[41] Using this set of anomalous fluids, we address a number of questions related to the features of the pair interaction, in addition to the two length scales, that control the temperature-pressure regime of the water-like liquid state anomalies versus the liquid-liquid critical point. Both the liquid-liquid critical point and the water-like anomalies require a change in the nature of local order in the liquid with density, and therefore two length scales in the case of core-softened fluids. The liquid-liquid critical point, however, depends on the energetic bias towards segregation of the two length scales with decreasing temperature. In contrast, the water-like liquid state anomalies require an excess entropy anomaly, involving a continuous transformation of the liquid from low- to high-density through a range of quasi-binary states reflecting the competition between two length scales in the intermediate regime.[18] In order to understand the relationship between the interaction potential, the water-like liquid state anomalies and the liquid-liquid critical point, it is therefore necessary to consider the temperature-dependent stabilization of the low- and high-density length scales as well as the density-dependent changes in the entropy of the system.

In order to understand how the change in interaction potential within the multi-Gaussian water models affects the thermodynamic and kinetic water-like anomalies, it is necessary to map out the excess entropy anomaly for the different model fluids. We use the pair correlation entropy as a simple structural estimator of the excess entropy, defining it for a one-component fluid of structureless particles as

$$\frac{S_2}{Nk_B} = -2\pi\rho \int_0^\infty \{g(r)\ln g(r) - [g(r)-1]\} r^2 dr, \qquad (1)$$

where $g(r)$ is the radial distribution function. It is typically the dominant contribution to the excess entropy of a fluid expressed as a multi-particle correlation expansion of the form

$$S_{\text{ex}} = S - S_{\text{id}} = S_2 + S_3 + \ldots, \qquad (2)$$

where S_n is the entropy contribution due to n-particle spatial correlations.[42–46] The excess entropy and mobility anomalies are linked by excess entropy scaling relations of the form

$$X^* = A\exp(\alpha(S_{\text{ex}}/Nk_B)), \qquad (3)$$

where X^* are dimensionless transport properties with either macroscopic (Rosenfeld) or microscopic (Dzugutov) reduction parameters and the scaling parameters, α and A, depend on the functional form of the underlying interactions.[47–50] In the case of simple liquids, the excess entropy scaling parameters can be approximately set as $A \approx 0.6$ and $\alpha \approx 0.8$. In addition, for such fluids, the pair correlation entropy per particle, s_2, typically represents $85\% - 90\%$ of the total excess entropy.[51] Mittal *et al.* investigated the approximation $S_{\text{ex}} \approx S_2$ as well as the relation between the excess entropy and the diffusion coefficient for the specific case of core-softened fluids.[20,22] They have shown that S_2 captures the most important and qualitative behaviors of S_{ex} with a reasonable quantitative accuracy.

As an additional means to relate the interaction potential to the liquid-state properties, we characterize the potential energy surface (PES) of the multi-Gaussian family of water-like liquids using instantaneous normal mode analysis. In the instantaneous normal mode (INM) approach, the key quantity is the ensemble-averaged curvature distribution of the PES sampled by the system. For a system of N particles, the mass-weighted Hessian associated with each instantaneous configuration is diagonalized to yield $3N$ normal mode eigenvalues and eigenvectors and the ensemble-average of this distribution is referred to as the INM spectrum. The INM spectrum of a liquid will have a substantial fraction of unstable modes with negative eigenvalues that simulations suggest is strongly correlated with the diffusivity.[52–57] Random energy models of liquids also suggest that for supercooled liquids there will be a connection between the fraction of imaginary modes, the diffusivity, and the configurational entropy.[58,59] Our previous work on INM analysis of a core-softened water-like fluid demonstrated that the instantaneous normal mode spectra carry significant information on the dynamical consequences of the interplay between length scales characteristic of anomalous fluids.[19] We have therefore performed an INM analysis of the multi-Gaussian water-like fluids to understand the relationship between the interaction potential, anomalies and the liquid-liquid critical point.

The paper is organized as follows. The computational details of the simulations and the equation of state data for the multi-Gaussian family of water models are summarized in Sec. II. Section III contains the results and the conclusions in Sec. IV.

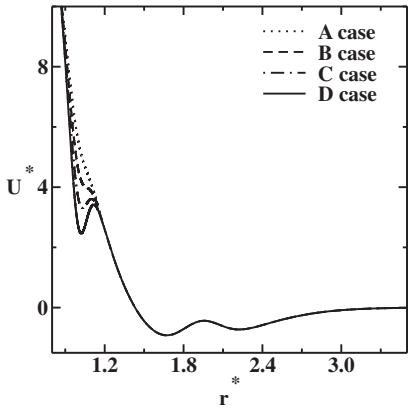

FIG. 1. Interaction potential obtained by changing parameters h_1 in Eq. (4). The potential and the distances are in dimensionless units $U^* = U/\gamma$ and $r^* = r/r_0$.

II. THE MODEL

A. The potential

The multi-Gaussian family of water-like fluids is defined by pair-additive, continuous, and core-softened interactions with the functional form

$$U(r) = \epsilon\left[\left(\frac{\sigma}{r}\right)^a - \left(\frac{\sigma}{r}\right)^b\right] + \sum_{j=1}^{4} h_j \exp\left[-\left(\frac{r-c_j}{w_j}\right)^2\right]. \tag{4}$$

The first term is a Lennard-Jones potential-like and the second one is composed of four Gaussians, each of width w_j centered at c_j. The potential and the distances are given in dimensionless units, $U^* = U/\gamma$ and $r^* = r/r_0$, where γ is the energy scale and r_0 is the length scale chosen so the closest approach between particles is about $r^* = 1$, i.e., so that the second length scale associated with the repulsive shoulder remains the same. Here we use $\epsilon/\gamma = 0.02$ and $\sigma/r_0 = 1.47$. Modifying h_1 in the Eq. (4) allows us to change the depth of the hard-core well, as illustrated in Fig. 1 while keeping the shape and location of the attractive well constant. We report here results for four different values for h_1 and they are expressed as a multiple of a reference value h_1^{ref} as shown in the Table I. For all the four cases the values of a, b, $\{c_j, w_j\}$ with $j = 1, \ldots, 4$, and h^{ref}. Table II gives the parameter values in Å and kcal/mol consistent with reproducing the oxygen-oxygen radial distribution of ST4 water using case D.[41]

TABLE I. Parameters h_1 for potentials A, B, C, and D.

Potential	Value of h_1
A	$0.25\,h_1^{ref}$
B	$0.50\,h_1^{ref}$
C	$0.75\,h_1^{ref}$
D	$1.00\,h_1^{ref}$

TABLE II. Parameters for potentials A, B, C, and D in units of Å and of kcal/mol.

Parameter	Value	Parameter	Value
a	9.056	w_1	0.253
b	4.044	w_2	1.767
ϵ	0.006	w_3	2.363
σ	4.218	w_4	0.614
c_1	2.849	h_1^{ref}	−1.137
c_2	1.514	h_2	3.626
c_3	4.569	h_3	−0.451
c_4	5.518	h_4	0.230

B. The simulation details

The properties of the system were obtained by NVT molecular dynamics using Nose-Hoover heat-bath with coupling parameter $Q = 2$. The system is characterized by 500 particles in a cubic box with periodic boundary conditions, interacting with the intermolecular potential described above. All physical quantities are expressed in reduced units and defined as

$$\begin{aligned} t^* &= \frac{t(m/\gamma)^{1/2}}{r_0} \\ T^* &= \frac{k_B T}{\gamma} \\ p^* &= \frac{p r_0}{\gamma} \\ \rho^* &= \rho r_0^3 \\ D^* &= \frac{Dm}{\gamma r_0^2}. \end{aligned} \tag{5}$$

Standard periodic boundary conditions together with predictor-corrector algorithm were used to integrate the equations of motion with a time step $\Delta t^* = 0.002$ and potential cut off radius $r_c^* = 3.5$. The initial configuration is set on solid or liquid state and, in both cases, the equilibrium state was reached after $t_{eq}^* = 1000$ (what is in fact 500 000 steps since $\Delta t^* = 0.002$) . From this time on the physical quantities were stored in intervals of $\Delta t_R^* = 1$ during $t_R^* = 1000$. The system is uncorrelated after $t_d^* = 10$, as judged from the velocity auto-correlation function. 50 decorrelated samples were used to get the average of the physical quantities.

At each state point, 100 configurations were sampled and used to construct the instantaneous normal mode spectra and associated quantities. We repeated the calculation for some state points using 500 configurations and found no significant difference.

C. Instantaneous normal modes analysis

The potential energy of configuration $\mathbf{r}$ near $\mathbf{r_0}$ can be written as a Taylor expansion of the form

$$U(\mathbf{r}) = U(\mathbf{r_0}) - \mathbf{F} \bullet \mathbf{z} + \frac{1}{2}\mathbf{r}^{\mathbf{T}} \bullet \mathbf{H} \bullet \mathbf{z}, \tag{6}$$

where $\mathbf{z_i} = \sqrt{m_i}(\mathbf{r_i} - \mathbf{r_0})$ are the mass-scaled position coordinates of a particle i. The first and second derivatives of $U(\mathbf{r})$ with respect to the vector $\mathbf{z}$ are the force and the Hessian matrix, denoted by $\mathbf{F}$ and $\mathbf{H}$, respectively. The eigenvalues of the Hessian $\mathbf{H}$ are $(\{\omega_i^2\}, i = 1, 3N)$ representing the squares of normal mode frequencies, and $\mathbf{W}(\mathbf{r})$ are the corresponding eigenvectors. In a stable solid, $\mathbf{r_0}$ can be conveniently taken as the global minimum of the potential energy surface $U(R)$, which implies that $\mathbf{F} = 0$ and $\mathbf{H}$ has only positive eigenvalues corresponding to oscillatory modes. The INM approach for liquids interprets $\mathbf{r}$ as the configuration at time t relative to the configuration $\mathbf{r_0}$ at time t_0. Since typical configurations, $\mathbf{r_0}$ are extremely unlikely to be local minima, therefore $\mathbf{F} \neq 0$ and $\mathbf{H}$ will have negative eigenvalues. The negative eigenvalue modes are those which sample negative curvature regions of the PES, including barrier crossing modes. The ensemble-averaged INM spectrum, $\langle f(\omega)\rangle$, is defined as

$$f(\omega) = \left\langle \frac{1}{3N} \sum_{i=1}^{3N} \delta(\omega - \omega_i) \right\rangle. \tag{7}$$

Quantities that are convenient for characterizing the instantaneous normal mode spectrum are: (i) the fraction of imaginary frequencies (F_i), defined as

$$F_i = \int_{im} f(\omega) d\omega, \tag{8}$$

and the Einstein frequency (ω_E), given by

$$\omega_E^2 = \int \omega^2 f(\omega) d\omega = \frac{\langle Tr\mathbf{H}\rangle}{m(3N-3)}, \tag{9}$$

where the integral is performed over the entire range of frequencies, real as well as imaginary.

III. RESULTS

A. Phase diagram

Figure 2 illustrates the pressure-temperature phase diagram for the four cases of the potential.[40] Because of the presence of the attractive interaction, all four cases have a liquid-gas transition with an associated critical point that is not shown here. In addition, all the four model liquids studied here have a liquid-liquid critical point. Cases A, B, and C have water-like density and diffusional anomalies. The solid bold lines represent the locus of temperatures of maximum density (TMD) for different isobars. State points enclosed by the TMD locus represent the regime of density anomaly within which $(\partial\rho/\partial T)_P > 0$. The maximum temperature along the TMD locus, denoted by $T_{TMD}^{\max}$, is the threshold temperature for onset of the density anomaly. The dotted-dashed lines are the temperatures of maximum and minimum diffusivity along different isotherms.[40]

This overall change in the nature of the liquid-state phase diagram for the four multi-Gaussian liquids is summarized in Figure 3. Clearly, as the second length scale shifts from an inflection point on the repulsive shoulder to a well with progressively increasing depth and curvature, the region of liquid state anomalies shrinks and disappears. The figure illustrates how the pressure and temperature associated the liquid-

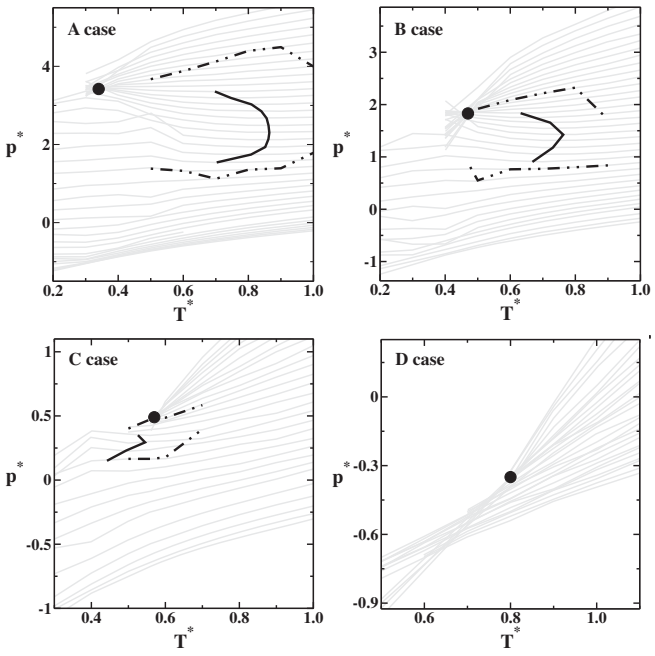

FIG. 2. Pressure-temperature phase diagram for cases A, B, C, and D. The thin solid lines are the isochores $0.30 < \rho^* < 0.65$. The liquid-liquid critical point is the dot, the locus of temperatures of maximum density is the solid thick line and the locus of diffusion extrema is the dot-dashed line.

gas and liquid-liquid critical points vary with the potentials A, B, C, and D. The same graph also shows that as the shoulder becomes deeper, the maximum temperature of the TMD locus, which marks the onset temperature for thermodynamically anomalous behavior, approaches the liquid-liquid critical point.

Since the thermodynamic and mobility anomalies of water are correlated, we first focus on understanding the thermodynamic condition for the presence of density anomaly. This may be stated as

$$\frac{\partial S}{\partial \rho} = -\frac{V^2 \alpha}{N K_T} > 0, \tag{10}$$

where α is the thermal expansion coefficient and K_T is the isothermal compressibility. For the system to have a large

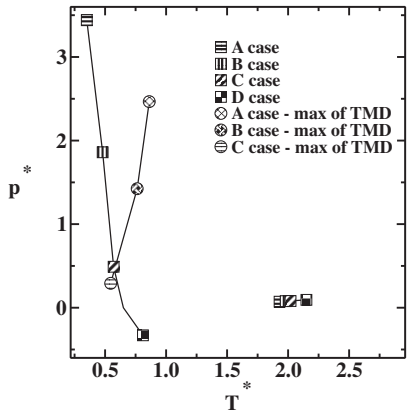

FIG. 3. Pressure versus temperature locations of liquid-liquid and liquid-gas critical points (squares), and the maximum temperature of the TMD locus (circles), for potentials A − D.

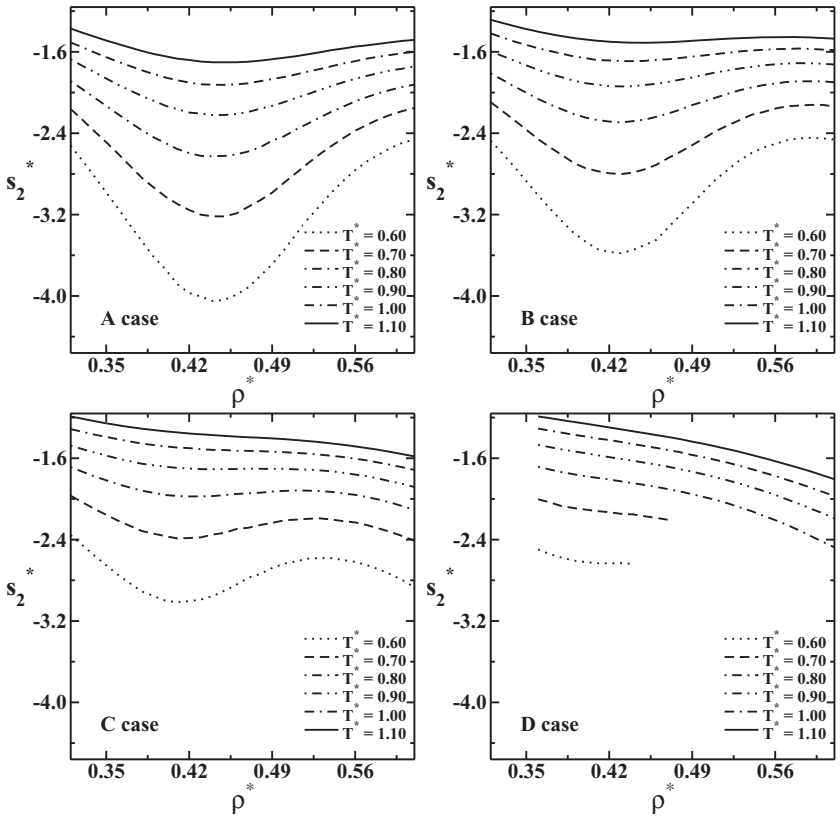

FIG. 4. Pair entropy versus density for the cases A, B, C, and D for various temperatures.

anomalous region, the ratio α/K_T should be therefore large and negative. Near the critical point, the compressibility, K_T, and thermal expansion coefficient, α_T, diverge, however the compressibility diverges with a large exponent making the ratio zero. In this case, the condition given by Eq. (10) cannot be fulfilled. This suggests that near the liquid-liquid critical point the system prefers to undergo a phase separation into high- and low-density liquids rather than show a smooth entropy anomaly.

B. Excess entropy and pair correlations

As discussed in Sec. III A, the density anomaly corresponds to a set of state points for which $(\partial S/\partial\rho)_T > 0$. The total entropy is a sum of the ideal ($S_{\rm id}$) and excess ($S_{\rm ex}$) contributions. Since $S_{\rm id}$ decreases monotonically with increasing density, therefore, a density anomaly must imply the presence of an excess entropy anomaly, $(\partial S_{\rm ex}/\partial\rho)_T > 0$. Errington *et al.* have further shown that the strength of the excess entropy anomaly required to give rise to density anomaly is given by the condition $\Sigma_{\rm ex} = [\partial(S_{\rm ex}/Nk_B)/\partial \ln\rho]_T > 1$.[22] By approximating the excess entropy with the two-body correlation contribution of s_2 (see Eq. (1)), we relate the structural information in the radial distribution function of the fluid to the thermodynamic behavior.

Figure 4 illustrates the $s_2^*(\rho) = S_2/Nk_B$ versus ρ^* for various temperatures and for the potentials A, B, C, and D. For cases A, B, and C, at low temperatures, there is a rise in excess entropy on isothermal compression characteristic of water-like liquids[11,19,20] that contrasts with the behavior of simple liquids where free volume arguments are sufficient to justify a monotonic decrease in entropy on isothermal compression. For the case D, no anomaly is observed in the pair entropy even at low temperatures. The progressive attenuation of the anomalies on going from case A to case *D*, is illustrated in Figure 5 which compares the behavior of the pair entropy versus density for all studied potentials at a given temperature, $T^* = 0.9$. This graph together with Figure 3 indicates that as the maximum temperature at the TMD line approaches the liquid-liquid critical temperature, the pair entropy curve becomes more flat and the anomalous behavior disappears.

The origin of the pair entropy anomaly in fluids with two length scales can be explained in terms of a competition between two length scales at intermediate densities. Only a

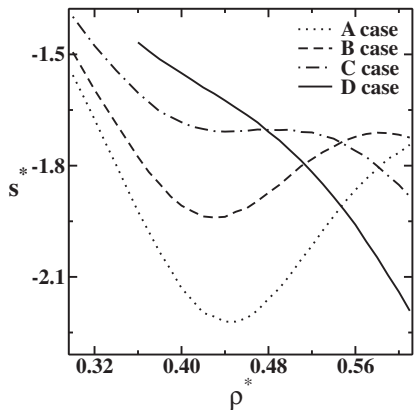

FIG. 5. Pair entropy versus density for the cases A, B, C, and D at $T^* = 0.9$.

single length scale dominates in the low- and high-density limits while at intermediate densities, where both length scales are present, can be regarded as quasi-binary systems with a mixing entropy. The radial distribution functions shown in our previous study clearly demonstrate the presence of two length scales. They also show that with the increasing temperature, the shorter length scale peak of $g(r)$ becomes more prominent in cases A, B, and C. In contrast, in the case D, both length scales associated with the first and second peak of the $g(r)$ broaden with increasing temperature as a consequence of which there is no emergence of an anomaly with decreasing temperature.

The crucial question to ask in the multi-Gaussian family of water models is why, despite the presence of two length scales at intermediate densities, the pair entropy anomaly is progressively lost as the shoulder goes from being an inflexion point to a minimum with about twice the depth as the outer, attractive well. Clearly the rise in entropy with isothermal compression due to the mixing of two length scales is counteracted by additional effects. To understand this we note that the entropy of an one-dimensional harmonic oscillator of frequency ω is given by

$$\frac{s_\omega}{Nk_B} = 1 - \ln(\beta\hbar\omega)\,. \tag{11}$$

The increasing curvature of the short-range minimum, relative to the attractive minimum, implies that a pair-separated trapped in the shoulder minimum will have lower vibrational entropy than one trapped in the broad shallow attractive minimum. As a consequence, at intermediate densities, while the presence of two length scales will increase entropy, the loss of entropy when the pairs are located in the short-range minimum will tend to decrease entropy. As the shoulder minimum becomes deeper, the second effect becomes more important and the excess entropy anomaly disappears. In systems such as the two-scale linear ramp, such curvature-dependent effects will be absent.

It is also interesting to consider the shifting of the liquid-liquid critical point to lower pressures and higher temperatures. For a temperature-driven phase separation into low-density liquid (LDL) and high-density liquid (HDL), increasing energetic stabilization of one length scale relative to the other is required. In case A, this is clearly due to the outer attractive well with a depth of about $\Delta U^* \approx 0.3$ and $T_c^* \approx 0.3$. In case D, this is due to the shorter length scale with a well depth of about $\Delta^* = 1.00$ and $T_c^* \approx 0.8$. For a shallow shoulder, the high density liquid is stabilized under high pressure. Within the HDL phase, particles are occupying the shoulder scale. The density anomalous region, characterized by having particles in the two scales occurs at the pressure range of the low density liquid phase. As the shoulder scale becomes deeper, less pressure is needed to form the high density liquid. The LDL phase occupies a smaller pressure range and, therefore, the density anomalous region shrinks. For a very deep shoulder well as in case D, the HDL requires no pressure to be formed, the LDL is at negative pressures and the anomalous density regime disappears.

C. Diffusion and Rosenfeld reduction parameter

Previously we have shown that the diffusion coefficient in the cases A, B, and C decreases with the decrease of the density for a certain range of densities.[40] The region in the pressure temperature phase diagram limited by the maxima and minima of the diffusion coefficient is illustrated as dot-dashed lines in Fig. 2. In the case D, the diffusion coefficient increases with the decrease of the density as in normal liquids. It is interesting to notice that the same behavior is also observed in the pair entropy suggesting that the anomalies present in these two quantities might be related. In order to check this hypothesis we now consider the scaling relationship between the diffusivity and the pair entropy. Using the Rosenfeld macroscopic reduction parameters for the length as $\rho^{-1/3}$ and the thermal velocity as $(k_BT/m)^{1/2}$, the dimensionless diffusivity is defined as

$$D_R \equiv D\frac{\rho^{1/3}}{(k_BT/m)^{1/2}}\,. \tag{12}$$

The scaling of the reduced diffusivity, D_R with pair entropy, s_2^* is illustrated in Fig. 6. Previous results for core-softened fluids suggest that $\Delta S = S_{ex} - S_2$ tends to be density dependent in anomalous fluids,[16] resulting in a stronger isochores dependence when $\ln(D_R)$ is plotted against S_2, rather than against S_{ex}. In the present study, we have computed only S_2 and, therefore, Fig. 6 shows scaling with respect to S_2. For case A, the collapse of data from all the state points on a single line is quite good. This case model very closely mimic those of the Gaussian-core fluid,[60] a system which also exhibits good scaling of Rosenfeld parameterized self diffusivity with two-body excess entropy. This makes logical sense since the case A and the Gaussian-core systems are qualitatively similar for low to intermediate temperatures. As we progress

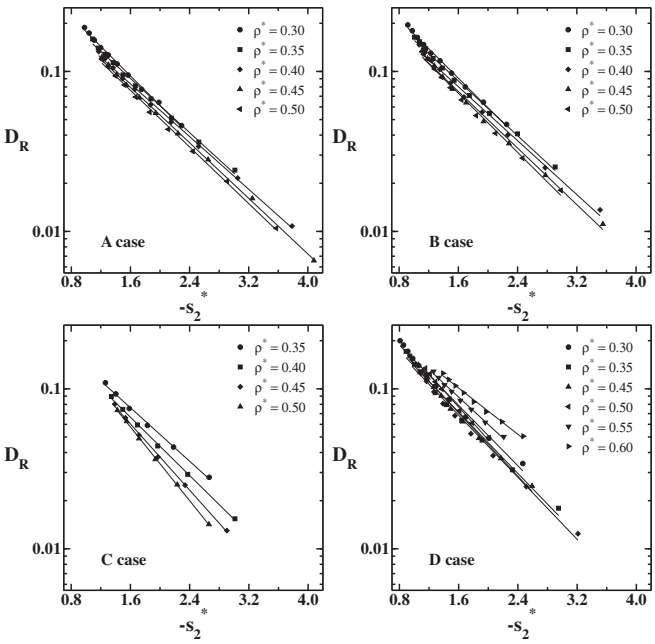

FIG. 6. Diffusion in Rosenfeld units as a function of $-s_2^*$ for the cases A, B, C, and D.

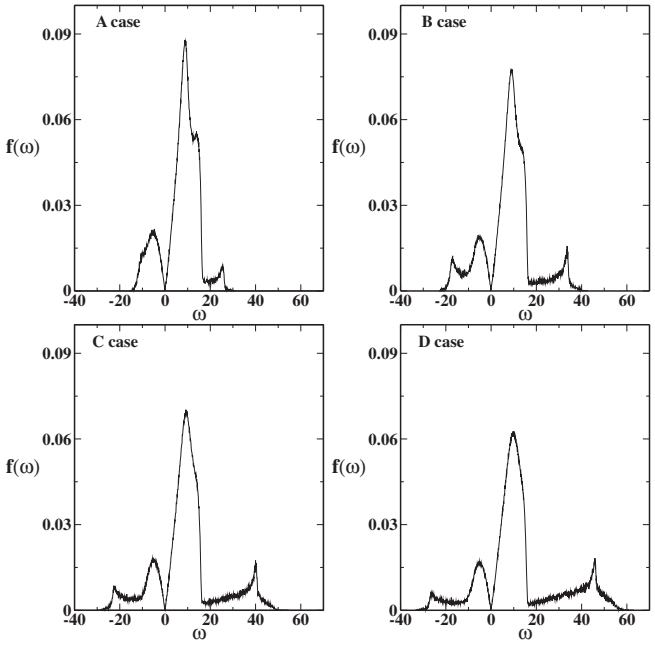

FIG. 7. Normal models versus frequency for the four studies cases. The density is fixed, $\rho^* = 0.50$ in all the cases and the temperature is varied.

from case A to case D, the isochores dependence of the scaling parameters becomes more pronounced suggesting that the density dependence of ΔS increases on going from case A to case D.

This is consistent with other anomalous systems that were studied recently. For liquid water, the D_R vs. s_2 scaling holds reasonably well for lower temperature state points (where anomalies are present), but it develops clear isochore dependence at high temperature (where anomalies disappear).[16,61] For core-softened liquids with short-range attractions the D_R vs. s_2 relationship holds well for the anomalous state points and breaks down for conditions when the anomalies disappear.[62–65]

D. The instantaneous normal mode spectrum

The variation in anomalous behavior in the multi-Gaussian family of water-like liquids studied here suggests that in addition to length scales, we need to look at other features of the pair potential, e.g., its first and second derivatives. Instantaneous normal mode analysis provides a way to summarize information on the curvature distribution of the potential energy landscape. In Figure 7, we show the INM spectra of liquids bound by the four potentials (A, B, C, and D) at a common state point of $\rho^* = 0.50$ and temperature $T^* = 0.8$. The crucial features are as follows:

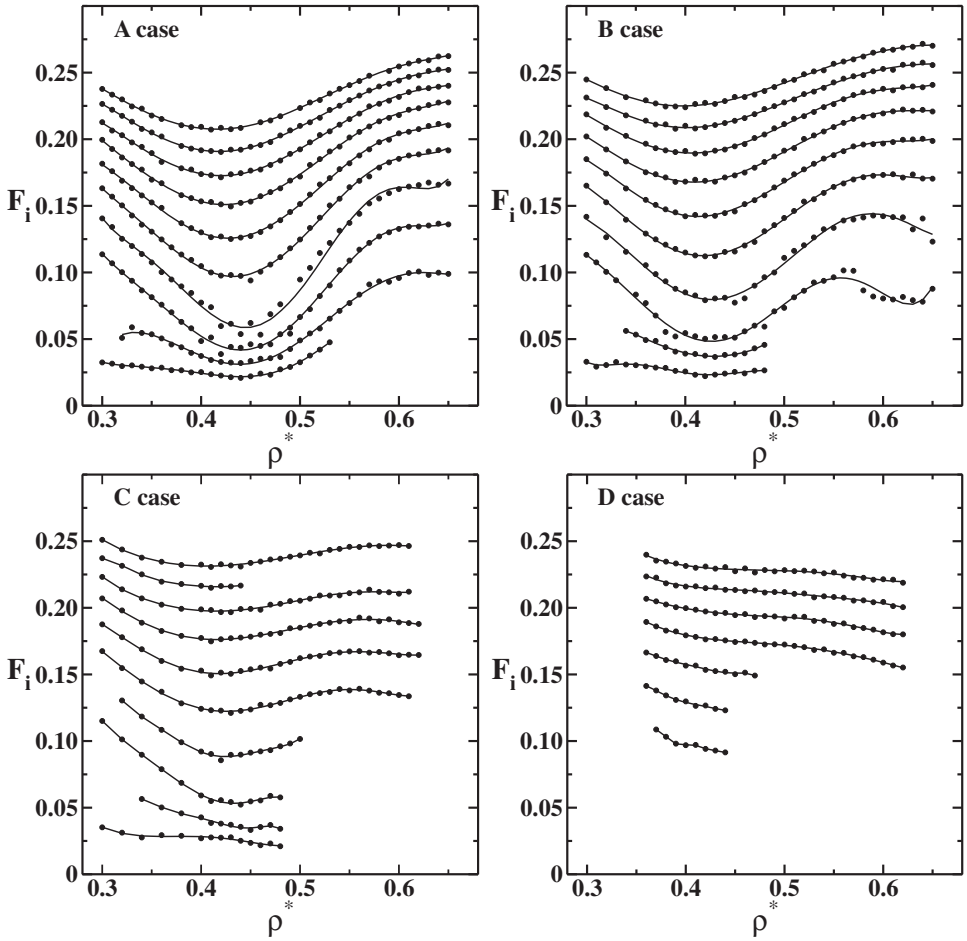

FIG. 8. Fraction of imaginary modes versus density for fixed temperatures, $T^* = 0.20$, 0.30, 0.40, 0.50, 0.60, 0.70, 0.80, 0.90, and 1.10 from bottom to top for cases A, B, and C. For case D temperature starts at $T^* = 0.50$.

- A low-frequency split peak in the real branch centered at about $\omega = 10$, that does not vary significantly between the four cases and must reflect modes associated with the outer attractive well;
- A high-frequency peak in the real branch, centered at approximately 30, 35, 40, and 50 for cases A, B, C, and D, respectively, which must correspond to motion in neighborhood of the shoulder length scale. As the curvature of the short-range minimum increases, this features shifts to higher frequencies and becomes more prominent; and
- The imaginary branch reflects regions of negative curvature in the neighborhood of barriers and inflection points. Case A, where there is no barrier in the pair interaction but only an inflection point has a single peak such as a simple liquid. However, this peak is broad because of the core-softened repulsive wall and the fraction of imaginary modes is large. As the barrier between the short and long length scales becomes more pronounced in the pair interaction, the second peak in the imaginary branch becomes more prominent.

Thus, the real branch is dominated by vibrational modes associated with motion in the attractive and shoulder length scales while the imaginary modes branch is dominated by negative curvature modes associated with transitions between the shoulder and attractive wells. For the case A, the real branch has three peaks related to the three basins: the shoulder scale, the attractive scale, and a second attractive scale located at further distance in Fig. 1. It has just one imaginary peak that indicating that transitions between the two length scales do not require local barrier crossing. For the cases B and C, the imaginary branch has two peaks suggestive of modes connecting between the shoulder scale, attractive scale, and second attractive scales. The peak with largest frequency in the real branch has larger frequency in the case C than in the case A and is related to the shoulder scale. For the case D, the shoulder is deep and so the frequency related to the shoulder scale has a very high frequency. The imaginary branch has two distinct oscillation modes that exclude transitions between the shoulder scale and the other scales and, therefore, no anomalies are expected.

The above discussion suggests that INM spectra carry fairly detailed information on the dynamics of transitions between the two length scales. The two features which are a compact signature of INM spectra are the Einstein frequency and the fraction of imaginary modes. Isotherms of the Einstein frequency as a function of density for all the four cases show a monotonic increase with density and do not show any significant signatures of the water-like anomalies. The fraction of imaginary modes, in contrast, correlates strongly with the anomalous behavior of the pair entropy and the diffusivity. Figure 8 shows the F_i curves versus density for various isotherms of all the four multi-Gaussian model fluids studied here. The parallel behavior of the $s_2(\rho)$ and $F_i(\rho)$ curves at corresponding isotherms is immediately obvious, though the $F_i(\rho)$ have a stronger non-monotonic behavior than $s_2(\rho)$ curves. This can be seen most clearly for a high-temperature isotherm.

IV. CONCLUSIONS

This paper examines the relationship between water-like anomalies and the liquid-liquid critical point in a family of model fluids with multi-Gaussian and core-softened pair interactions. The pair interaction in this family of liquids is composed of a sum of Lennard-Jones and Gaussian terms, in such a manner that the longer length scale associated with a shallow, attractive well is kept constant while the shorter length scale associated with the repulsive shoulder changes from an inflection point to a minimum of progressively increasing depth. The maximum depth of the shoulder length scale is chosen so that the resulting potential reproduces the oxygen-oxygen radial distribution function of the ST4 model of water. As the energetic stabilization of the shoulder length scale increases, the liquid-liquid critical point shifts to higher temperatures and lower pressures. Simultaneously, the temperature for onset of the density anomaly decreases and the region of liquid state anomalies in the pressure-temperature plane diminishes. The condition for the presence of anomalies is inconsistent with divergences near a critical point, so that in the limiting case of maximum shoulder well depth, the anomalies disappear.

To understand our results for the phase diagram and liquid-state anomalies of the multi-Gaussian family of water-like fluids, it is important to note that, in addition to the presence of two length scales, it is necessary to consider the energetic and entropic effects as determined by local minima and curvatures of the pair interaction. As the shoulder depth increases, the pressure required to form the high density liquid decreases and the temperature up to which the high-density liquid is stable increases. This explains the shift of the liquid-liquid critical point to much lower pressures and higher temperatures. To understand the entropic effects associated with the changes in the interaction potential, we computed the pair correlation entropy and demonstrated the attenuation of the excess entropy anomaly as the shoulder length scale changed from an inflection point to a deep minimum. In conjunction with Rosenfeld-scaling of transport properties, this is consistent with the progressive loss of water-like thermodynamic, structural, and transport anomalies. The excess entropy anomaly in two-scale, isotropic fluids is due to a rise in entropy as a result of competition between two length scales at intermediate densities. In the case of continuous potentials, the vibrational entropy associated with the two length scales becomes important. To index the overall curvature distribution in the liquid, we have used instantaneous normal mode analysis and shown the fraction of imaginary frequency modes correlates well with the anomalous behavior of the diffusivity and the pair correlation entropy. A detailed analysis of the INM spectrum shows that as the shoulder well increases in depth, there is a simultaneous rise in the positive curvature associated with the shoulder minimum as well as the negative curvature of the barrier separating the shoulder minimum from the attractive minimum. Consequently, the vibrational entropy associated with pairs of particles separated by the shoulder distance decreases, relative to that of pairs trapped in the outer attractive well. Therefore, the mixing entropy due to the presence of two length scales is counteracted by the

changes in vibrational entropy associated by the two length scales.

A general conclusion that emerges from this study is that even though the ratio between the two length scales is important for locating the temperature range of the anomalies,[66] additional energetic and entropic effects associated with local minima and curvatures of the pair interaction can play an important role. The liquid-liquid phase separation depends on the relative energies associated with the two length scales whereas the water-like anomalies depend upon a continuous rise in entropy as a function of isothermal compression. A number of recent studies of core-softened fluids illustrate this conclusion. For example, energetic and entropic effects play a very different role in the discrete and discontinuous versions of the shouldered well potential.[18] In the discrete case, the enthalpic implications do not change significantly and the liquid-liquid critical point is not significantly different in the two systems. In contrast, the continuous potential allows for a smooth transformation through a range of quasi-binary states from low- to high-density and shows water-like anomalies. A more recent study of core-softened fluids shows that increasing the depth of the attractive well,[67] while leaving the shoulder feature constant, results in disappearance of the anomalies while shifting the liquid-liquid critical point to lower pressures and higher temperatures.

ACKNOWLEDGMENTS

This work is supported by the Indo-Brazil Cooperation Program in Science and Technology of the CNPq (Brazil) and DST (India). This work is also partially supported by the CNPq through the INCT-FCx.

[1] O. Mishima and H. E. Stanley, Nature (London) **396**, 329 (1998).
[2] K. A. Dill, T. M. Truskett, V. Vlachy, and B. Hribar-Lee, Annu. Rev. Biophys. Biomol. Struct. **34**, 173 (2005).
[3] P. Kumar, G. Franzese, and H. Eugene Stanley, J. Phys. Condens Matter **20**, 244114 (2008).
[4] J. D. Bernal and B. H. Fowler, J. Chem. Phys. **1**, 515 (1933).
[5] H. Thurn and J. Ruska, J. Non-Cryst. Solids **22**, 331 (1976).
[6] See http://periodic.lanl.gov/default.htm, 2007 for periodic table of the elements.
[7] G. E. Sauer and L. B. Borst, Science **158**, 1567 (1967).
[8] S. J. Kennedy and J. C. Wheeler, J. Chem. Phys. **78**, 1523 (1983).
[9] T. Tsuchiya, J. Phys. Soc. Jpn. **60**, 227 (1991).
[10] C. A. Angell, R. D. Bressel, M. Hemmatti, E. J. Sare, and J. C. Tucker, Phys. Chem. Chem. Phys. **2**, 1559 (2000).
[11] R. Sharma, S. N. Chakraborty, and C. Chakravarty, J. Chem. Phys. **125**, 204501 (2006).
[12] P. H. Poole, M. Hemmati, and C. A. Angell, Phys. Rev. Lett. **79**, 2281 (1997).
[13] H. Tanaka, Phys. Rev. B **66**, 064202 (2002).
[14] M. Agarwal, R. Sharma, and C. Chakravarty, J. Chem. Phys. **127**, 164502 (2007).
[15] M. Agarwal and C. Chakravarty, J. Phys. Chem. B **111**, 13294 (2007).
[16] M. Agarwal, M. Singh, R. Sharma, M. P. Alam, and C. Chakravarty, J. Phys. Chem. B **114**, 6995 (2010).
[17] M. Agarwal, M. P. Alam, and C. Chakravarty, J. Phys. Chem. B **115**, 6935 (2011).
[18] A. B. de Oliveira, P. A. Netz, T. Colla, and M. C. Barbosa, J. Chem. Phys. **124**, 084505 (2006).
[19] A. B. de Oliveira, E. Salcedo, C. Chakravarty, and M. C. Barbosa, J. Chem. Phys. **132**, 234509 (2010).
[20] J. Mittal, J. R. Errington, and T. M. Truskett, J. Chem. Phys. **125**, 076102 (2006).
[21] J. Mittal, J. R. Errington, and T. M. Truskett, J. Phys. Chem. B **110**, 18147 (2006).
[22] J. R. Errington, T. M. Truskett, and J. Mittal, J. Chem. Phys. **125**, 244502 (2006).
[23] Z. Yan, S. V. Buldyrev, and H. E. Stanley, Phys. Rev. E **78**, 051201 (2008).
[24] R. Sharma, M. Agarwal, and C. Chakravarty, Mol. Phys. **106**, 1925 (2008).
[25] A. B. de Oliveira, G. Franzese, P. A. Netz, and M. C. Barbosa, J. Chem. Phys. **128**, 064901 (2008).
[26] P. H. Poole, F. Sciortino, U. Essman, and H. E. Stanley, Nature (London) **360**, 324 (1992).
[27] P. C. Hemmer and G. Stell, Phys. Rev. Lett. **24**, 1284 (1970).
[28] E. A. Jagla, Phys. Rev. E **58**, 1478 (1998).
[29] G. Franzese, G. Malescio, A. Skibinsky, S. V. Buldyrev, and H. E. Stanley, Nature (London) **409**, 692 (2001).
[30] M. R. Sadr-Lahijany, A. Scala, S. V. Buldyrev, and H. E. Stanley, Phys. Rev. Lett. **81**, 4895 (1998).
[31] A. B. de Oliveira, M. C. Barbosa, and P. A. Netz, Physica A **386**, 744 (2007).
[32] A. B. de Oliveira, P. A. Netz, and M. C. Barbosa, Euro. Phys. J. B **64**, 481 (2008).
[33] A. B. de Oliveira, P. A. Netz, and M. C. Barbosa, Europhys. Lett. **85**, 36001 (2009).
[34] A. B. de Oliveira, E. B. Neves, C. Gavazzoni, J. Z. Paukowski, P. A. Netz, and M. C. Barbosa, J. Chem. Phys. **132**, 164505 (2010).
[35] S. Prestipino, F. Saija, and G. Malescio, J. Chem. Phys. **133**, 144504 (2010).
[36] S. Zhou, Phys. Rev. E **77**, 041110 (2008).
[37] S. Zhou, J. Chem. Phys. **132**, 194112 (2010).
[38] S. A. Egorov, J. Chem. Phys. **128**, 174503 (2008).
[39] O. Pizio, Z. Sokolowska, and S. Sokolowski, Condens. Matter Phys. **14**, 174504 (2011).
[40] N. M. Barraz, E. Salcedo, and M. C. Barbosa, J. Chem. Phys **131**, 094504 (2009).
[41] T. Head-Gordon and F. H. Stillinger, J. Chem. Phys. **98**, 3313 (1993).
[42] H. S. Green, *The Molecular Theory of Fluids* (North-Holland, Amsterdam, 1952).
[43] R. E. Nettleton and H. S. Green, J. Chem. Phys. **29**, 1365 (1958).
[44] H. J. Ravache, J. Chem. Phys. **55**, 2242 (1971).
[45] D. C. Wallace, J. Chem. Phys. **87**, 2282 (1987).
[46] A. Baranyai and D. J. Evans, Phys. Rev. A **40**, 3817 (1989).
[47] Y. Rosenfeld, Phys. Rev. A **15**, 2545 (1977).
[48] Y. Rosenfeld, Chem. Phys. Lett. **48**, 467 (1977).
[49] Y. Rosenfeld, J. Phys. Condens. Matter **11**, 5415 (1999).
[50] M. Dzugutov, Nature (London) **381**, 137 (1996).
[51] A. Baranyai and D. J. Evans, Phys. Rev. A **42**, 849 (1990).
[52] P. Shah and C. Chakravarty, J. Chem. Phys. **115**, 8784 (2001).
[53] P. Shah and C. Chakravarty, J. Chem. Phys. **116**, 10825 (2002).
[54] P. Shah and C. Chakravarty, Phys. Rev. Lett. **88**, 255501 (2002).
[55] M. Cho, G. R. Fleming, S. Saito, I. Ohmine, and R. M. Stratt, J. Chem. Phys. **100**, 6672 (1994).
[56] E. L. Nave, A. Scala, F. W. Starr, H. E. Stanley, and F. Sciortino, Phys. Rev. Lett. **84**, 4605 (2000).
[57] M. C. C. Ribeiro and P. A. Madden, J. Chem. Phys. **106**, 8616 (1997).
[58] T. Keyes, Phys. Rev. E **62**, 7905 (2000).
[59] T. K. Keyes, J. Chowdhary, and J. Kim, Phys. Rev. E **66**, 051110 (2002).
[60] W. P. Krekelberg, T. Kumar, J. Mittal, J. R. Errington, and T. M. Truskett, Phys. Rev. E **79**, 031203 (2009).
[61] R. Chopra, T. M. Truskett, and J. R. Errington, J. Phys. Chem. B **114**, 10558 (2010).
[62] W. P. Krekelberg, J. Mittal, V. Ganesan, and T. M. Truskett, J. Chem. Phys. **127**, 044502 (2007).
[63] W. P. Krekelberg, J. Mittal, V. Ganesan, and T. M. Truskett, Phys. Rev. E **77**, 041201 (2008).
[64] Y. D. Fomin, V. N. Ryzhov, and N. V. Gribova, Phys. Rev. E **81**, 061201 (2010).
[65] Y. D. Fomin and V. N. Ryzhov, Phys. Lett. A **375**, 2181 (2011).
[66] Z. Yan, S. V. Buldyrev, P. Kumar, N. Giovambattista, P. G. Debenedetti, and H. E. Stanley, Phys. Rev. E **76**, 051201 (2007).
[67] J. da Silva, E. Salcedo, A. B. de Oliveira, and M. C. Barbosa, J. Chem. Phys. **133**, 244506 (2010).